Characterization of $Mn_{0.67}Zn_{0.33}Fe_2O_4$ nanoparticles synthesized under different pH

Rodrigo U. Ichikawa[1,a], Walter K. Yoshito[1,b], Margarida J. Saeki[2,c], Willian C. A. Maranhão[1,d], Fátima Goulart[1,e] and Luis G. Martinez[1,f]

[1]*Instituto de Pesquisas Energéticas e Nucleares, Av. Prof. Lineu Prestes, 2242 - Cidade Universitária, São Paulo - SP, 05508-000, Brasil.*

[2]*Instituto de Biociências, Universidade Estadual Paulista "Júlio de Mesquita Filho", Distrito de Rubião Junior, s/n, Botucatu - SP, 18618-970, Brasil.*

[a]*richikawa@ipen.br,* [b]*wyoshito@ipen.br,* [c]*mjsaeki@ibb.unesp.br,* [d]*willian.maranhao@gmail.com,* [e]*amitafis@hotmail.com,* [f]*lgallego@ipen.br*

Keywords: Mn-Zn ferrite nanoparticles, X-ray diffraction, thermogravimetric analysis, differencial thermal analysis, dynamic light scattering, scanning electron microscopy.

Abstract. Nanometric Mn-Zn ferrites were synthesized through co-precipitation technique using different pH's for the aqueous solution. The samples were characterized using X-ray diffraction, X-ray fluorescence, thermogravimetric analysis, differential thermal analysis, dynamic light scattering and scanning electron microscopy techniques. Monophasic nanoparticles were formed when a pH of 10.5 was used. This sample was analyzed Rietveld refinement of XRD data for determining its microstructural features. Mean crystallite sizes and microstrains were determined from XRD Line Profile Analysis by using Single-Line and Warren-Averbach methods. Crystallite sizes distribution was determined using lognormal distribution. Size-strain analysis methods agreed and showed that the obtained material is nanostructured and presents negligible microstrain.

Introduction

Manganese-zinc ferrites are key technological materials due to their unique properties, such as high initial magnetic permeability, high resistivity and low hysteresis loss [1,2]. These spinel ferrites are being increasingly used in electrical and magnetic applications, such as power transformers in electronics, rod antennas and information storage systems [3]. More recently nanostructured Mn-Zn ferrites are also being applied in medical procedures, like in diagnosis as magnetic carriers for bioseparation, enzymes and proteins immobilization [1]. Thus, its characterization regarding its crystal structure, microstructure and its behavior under temperature changes are of utmost importance. In the present work Mn-Zn ferrite nanoparticles were synthesized by the co-precipitation method, using different pH's for the precipitating solution and characterized by X-ray powder diffraction (XRD), X-ray fluorescence (XRF), thermal analysis (TA), dynamic light scattering (DLS) and scanning electron microscopy (SEM) techniques.

The crystal structure was modeled using Rietveld analysis of XRD data and microstructure characterization was performed by XRD line-profile analysis employing the so called Single-Line [4] and Warren-Averbach [5] methods for determination of mean crystallite sizes and microstrains. Chemical analysis was performed using energy-dispersive XRF spectroscopy. Thermal analyses were performed by means of Thermogravimetric (TG) and Differential Thermal Analysis (DTA) up to 1200°C. Particle size distributions were determined using dynamic light scattering.

Experimental Procedure

$Mn_{0.75}Zn_{0.25}Fe_2O_4$ nanocrystals were synthesized by wet chemical co-precipitation method, using analytical grade manganese chloride tetrahydrate ($MnCl_2.4H_2O$), zinc chloride ($ZnCl_2$) and iron chloride hexahydrate ($FeCl_3.6H_2O$) as starting materials. All the salts were dissolved in de-ionized water to obtain Fe^{3+}, Mn^{2+} and Zn^{2+} ions in aqueous solution. This solution was precipitated in three different basic aqueous solutions, with varying the concentration of sodium hydroxide (NaOH). For each solution a suitable amount of sodium hydroxide was used to obtain the desired pH (9.5; 10.5 and 12.0). Co-precipitation reactions were carried out adding (dropping) the mixed metal chlorides (heated at 95°C) into vigorously stirred NaOH solution. The resulting precipitates were vacuum-filtered and washed with distilled water to remove Cl^- ions. The resulting powders were oven-dried at 70°C for 24 hours, resulting in three different samples.

The samples were characterized by thermal analysis (thermobalance Setaram Labsys Instrumentation, TG-DTA/DSC, EUA) under dynamic air and heating rate of $10°C.min^{-1}$. All experiments were performed in alumina crucible.

The data of the particle size distribution were obtained by dynamic light scattering (ZetaPALS-Zeta Potential Analyzer, BrookHaven Corp.). The suspensions were prepared with 0.1% w / w solid to first measure and other measurements were diluted in 50% after the first measurement. The dilution was performed until a constant value of particle size distribution.

X-ray diffraction data were collected (Rigaku Ultima IV diffractometer) with Bragg-Brentano geometry, 285 mm goniometer radius, equipped with a pyrolytic graphite diffracted-beam monochromator, and $Cu_{K\alpha}$ radiation at 40 kV and 30 mA. The measurements were performed in the 2θ range from 10° to 100°, at 0.02° steps and 20 sec/step counting time. The divergence, antiscatter and receiving slits were set to 1/2°, 1/2° and 0.3 mm, respectively. X-ray fluorescence measurement was performed with a Shimadzu EDX-720 Spectrometer using 50 kV and 100 mA with a 1.0 mm beam.

Methods

X-ray diffraction line-profile analysis was used to study the microstructure of the nanoparticles, namely crystallite sizes and its distribution and microstrains. Structural parameters were refined by the Rietveld method using the program TOPAS Version 4.2 [6].

Mean crystallite sizes and microstrains were determined using Single-Line (SL) method as proposed by de Keijser et al. [4] and Warren-Aberbach (WA) methods [5]. These methods provide different mean crystallite size estimations. SL provides a volume-weighted value and WA an area-weighted value. This approach is very useful since the crystallite sizes distribution can be determined using both results [7]. For perform this it is necessary to assume that the crystallite size follow a lognormal distribution and the crystallites have spherical or cubic shape.

Results and Discussion

The agglomerate size distribution curves of Mn-Zn ferrite nanoparticles synthesized with pH 9.5, 10.5 and 12.0 can be seen in Fig. 1. The cumulative agglomerate sizes ($D_{10,}$ D_{50} and D_{90}), presented in Tab. 1, show that the agglomerate sizes increase with pH. This may be an indication that the pH of the precipitation solution can influence the surface properties of the material.

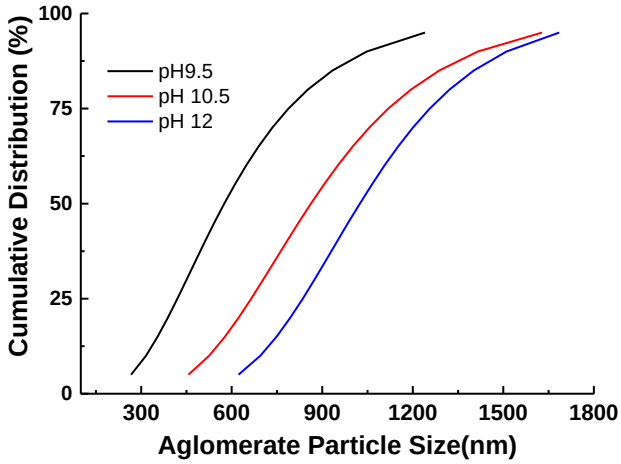

Figure 1 – Agglomerate *size distribution of Mn-Zn ferrites with different pH's co-precipitation.*

Table 1 – Cumulative agglomerate size distribution of the MnZn-ferrite synthesized in pH 9.5, 10.5 and 12.0.

pH	9.5	10.5	12.0
D_{10} [nm]	320	527	697
D_{50} [nm]	575	863	1024
D_{90} [nm]	1052	1430	1522

In Fig. 2 are presented the X-ray diffraction profiles for the three samples synthesized at different pH's.

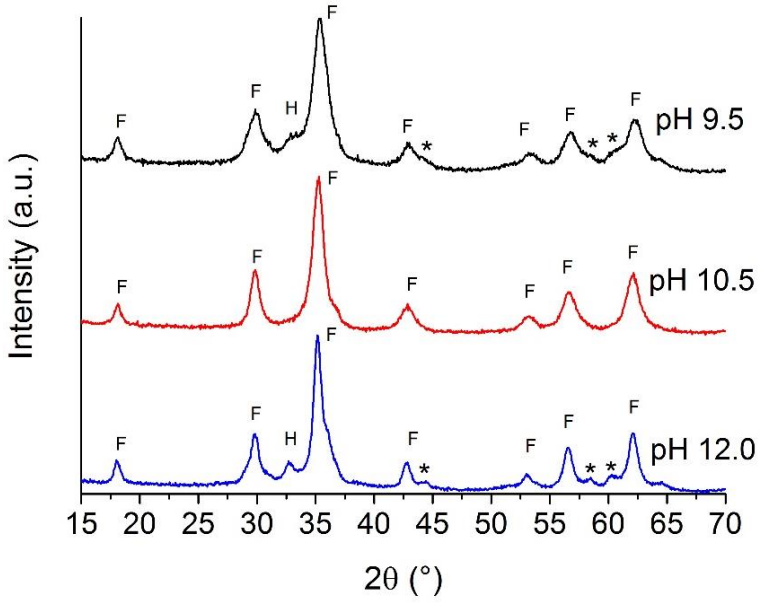

*Figure 2 – X-ray diffraction profiles for the three samples of Mn-Zn ferrites synthesized at different pH's. F stands for $Mn_{0.75}Zn_{0.25}Fe_2O_4$, H for α-$Fe_2O_3$ and * for non-identified phases.*

From Fig. 2 it can be seen that all the samples present mainly the desired spinel ferrite phase (peaks indicated as F). However, secondary phases were found for the samples synthesized at pH 9.5 and 12.0; α-Fe_2O_3 (peaks indicated as H) and also unidentified phases. These unidentified peaks (indicated as *) can be related to either Fe or FeO phases, however as some peaks of these phases are superimposed to the main phase ($Mn_{0.75}Zn_{0.25}Fe_2O_4$) the identification is hampered. Hence, the subsequent analysis was performed only for the monophasic sample synthesized at pH 10, since peaks of secondary phases can influence the results.

The lattice parameter was obtained by XRD data Rietveld refinement for the sample synthesized with pH 10 is presented in Tab. 2 with the refinement.quality factor Rwp. The value in brackts is the variance of the refined value.

Table 2 - Lattice parameter determined by XRD data Rietveld refinement and refinement quality factor Rwp.

Lattice parameter (nm)	**Rwp (%)**
0.8442 (3)	5.1

Using a plot of lattice parameter versus the Zn concentration from a study done by Rath [8], presented in Fig. 3, for comparing to the lattice parameter determined by Rietveld refinement (red point), we can infer the Zn content of this sample as being about 0.33, which is compatible to the value determined by XRF, which provided a value of 0.28.

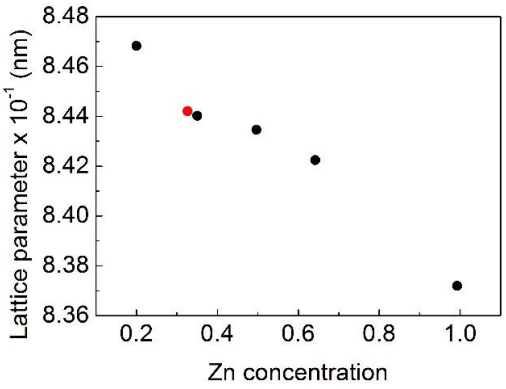

Figure 3 – Lattice parameter versus Zn concentration: In black: values from the study done by Rath [7]; in red: value obtained for the Mn-Zn ferrite in this study.

Mean crystallite sizes were determined using Single-Line and Warren-Averbach methods for the 022 and 044 reflections, since they were the most isolated and intense XRD reflections and the Warren-Averbach method needs at least two reflections of parallel planes. The mean crystallite size given by the Single-Line method is a volume-weighted value (Lv) while the Warren-Averbach method provides the area-weighted (La) one. The mean crystallite sizes and root mean square strain (RMSS) results are presented in Tab. 3.

Table 3 – Area (La) and volume (Lv) weighted mean crystallite sizes and root mean square strain for Mn-Zn ferrite synthesized with pH 10.5.

La (nm)	Lv (nm)	RMSS (10^{-3})
8.7 (5)	11.1 (3)	5.1

Using both, the volume-weighted and area-weighted mean crystallite sizes (Lv and La) it is possible to determine the crystallite sizes distribution [7]. For this study it was considered crystallites with spherical morphology and a lognormal distribution. In Fig. 4 is presented the crystallite size distribution. The crystallite size distribution reveals a narrow dispersion of crystallite sizes, with a mean men value of 10.1 nm and with a standard deviation of 3.7 nm.

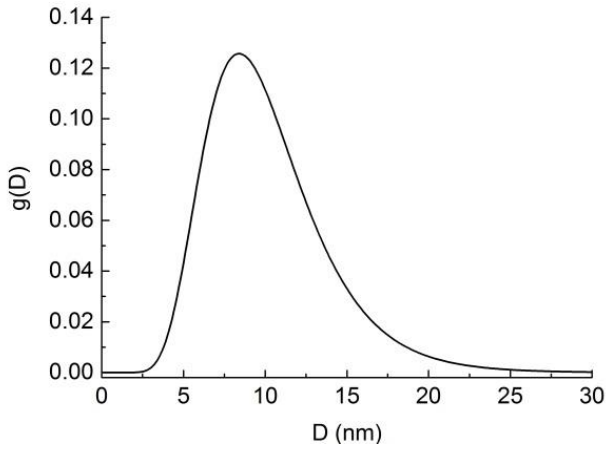

Figure 4 - Crystallite size distribution for the sample obtained with pH 10.5.

A thermal analysis study was performed on the sample in order to determine the temperatures at which transformations occur. In Fig. 5 are shown the TG and DTA curves. The thermogravimetric evolution from ambient temperature to 1200°C is similar for all the samples and shows a continuous decreasing corresponding to the water loss. DTA curve shows an endothermic process up to 100°C (water loss) and an exothermic one from 100° C to 200°C (decomposition of hydroxides). The peak at about 325°C corresponds to the oxidation of unreacted species, which is corroborated by the inflexion of the TGA curve, i.e. the incorporation of oxygen atoms. Between 1130°C and 1200°C occurs the dissociation of secondary phases and recrystallization of the MnZn-ferrite [1] as evidenced by XRD measurements shown in Fig. 8.

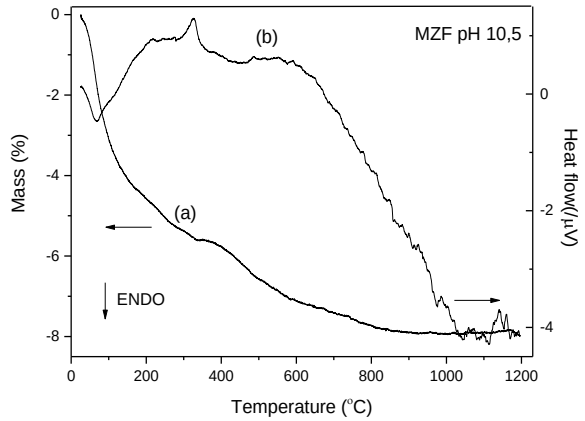

Figure 5 – Thermal analysis, TG (a) and DTA (b) in air atmosphere synthesized using pH 10.5.

Following this analysis the sample was heat-treated at 280°C, 480°C and 800°C in air and analyzed again for agglomerate sizes and distributions. The results for cumulative distribution are presented in Fig. 6. Results for agglomerate size (AS), polydispersity index (PI) and half width (HW) for samples heat-treated at 280°C, 480°C and 800°C are summarized Tab. 4.

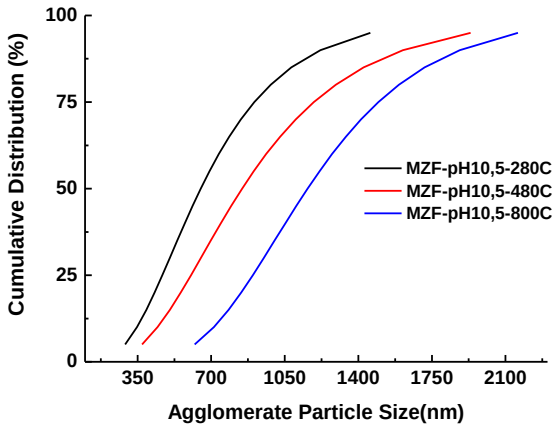

Figure 6 – Particle size distribution of Mn-Zn ferrite with heat-treatment temperature

Table 4 - Agglomerate size (AS), polydispersity index (PI) and half width (HW) of MnZn-ferrite synthesized with pH 10.5 and heat-treated at 280°C, 480°C and 800°C.

Sample	AS (nm)	PI	HW (nm)
280°C	654	0.280	365.0
480°C	852	0.277	458.9
800°C	1159	0.184	441.0

The heat-treated samples were analyzed by SEM. The micrographs presented in Fig. 7 show two different agglomerates for samples calcined at 280°C and 800°C formed two soft agglomerates and it was observed that the agglomerate sizes don't increase with increasing temperature, between 280°C and 800 °C. However the sample calcined at 1200°C contain hard agglomerates with larger sizes due to the powder sintering.

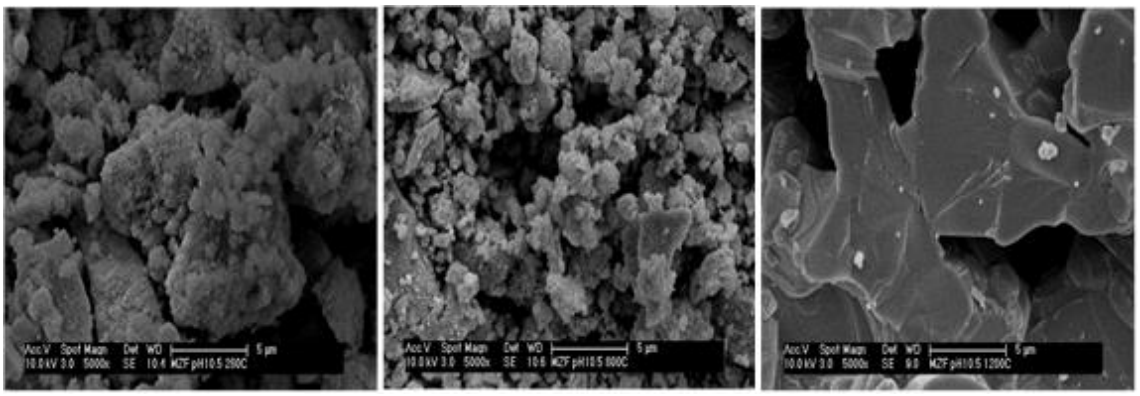

Figure 7 - SEM of the Mn-Zn ferrite powders heat-treated at: (a) 280°C, (b) 800°C and (c) 1200°C.

The X-ray diffraction profiles for the as-synthesized and heat- treated Mn-Zn ferrite samples are presented in Fig. 8. It can be observed that the heat treatments at 280°C, 480°C and 800° C was not effective for dissociate the secondary phase, although at 800° C can be observed a crystallite growth, evidenced by the narrowing of peaks. At this temperature is observed the presence of small amount of a phase identified as α-Fe_2O_3 which is not present when the sample was heat treated at 1200°C. This can be attributed to the dissolution of α-Fe_2O_3 and reduction of ferric ions at higher temperatures [1,8]. Some samples presented also a small contamination of SiO_2, probably formed due to residuals from the experimental apparatus used in the synthesis. For the sample heat-treated at 1200°C the only phase observed is the cubic spinel-ferrite well crystallized.

Rietveld analysis of XRD data was performed for determine cell parameters, phase density and unit cell volume for the as-synthesized (AS) and heath-treated samples. The results are presented in Tab. 5.

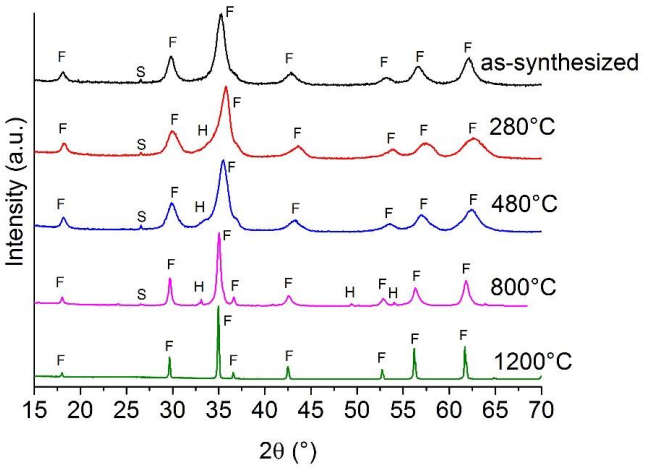

Figure 8 - XRD profiles for the as-synthesized and heat-treated MnZn-ferrite samples obtained using pH 10.5. F stands for $Mn_{0.75}Zn_{0.25}Fe_2O_4$, S for SiO_2 and H for α-Fe_2O_3.

Table 5 – Cell parameters (a), density (ρ_{XRD}) and unit cell volume determined by Rietveld refinement of XRD data.

Sample	a (nm)	ρ_{XRD} (g/cm^3)	V (nm^3)
AS	0.8436 (4)	5.166 (7)	0.6004 (9)
280°C	0.8392 (3)	5.230 (6)	0.5910 (6)
480°C	0.8419 (3)	5.180 (5)	0.5967 (6)
800°C	0.8470 (4)	5.087 (7)	0.6076 (9)
1200°C	0.8490 (1)	5.063 (2)	0.6120 (2)

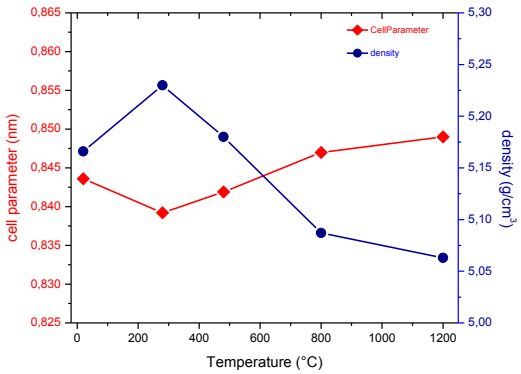

Figure 9 – Evolution of cell parameter and density for Mn-Zn ferrite as a function of heath-treatment temperature.

It can be observed a slight decrease in cell parameter and increase in density from the as-sinthesized sample to the treated at 280°C. This can be atributed to the elimination of hydroxides and starting of the crystallization, as confirmed by the exothermic peak at 280°C in the DTA curve. From 280°C to 1200°C is observed a continuous increase of cell parameter and decrease of density.

Conclusions

It was possible to conclude that the pH of 10.5 is the better choice to obtain monophasic Mn-Zn ferrite nanoparticles. From an extrapolation using the lattice parameter obtained by Rietveld refinement, the Mn-Zn ferrite composition was estimated as $Mn_{0.67}Zn_{0.33}Fe_2O_4$. The nanosized particles were successfully obtained as confirmed by size-strain analysis using Single-Line and Warren-Averbach methods. Size distribution presented a narrow dispersion around 10 nm. The mean agglomerate sizes always presented an increase for increasing pH and heat-treatment temperatures. The heat-treatment at 800°C revealed a formation of small amount of α-Fe_2O_3 which is dissolved by the reduction of ferric ions for the sample treated at 1200°C.

Acknowledgments

R. U. Ichikawa acknowledges CAPES and CNPq financial support. Dr[a]. Vera L. R. Salvador is acknowledged for helping in the X-ray fluorescence analysis. IPEN microscopy laboratory is highly acknowledged for the SEM images. IPEN Rheology laboratory and IPEN Fuel Cell and Hydrogen Center are also acknowledged.

References

[1] P. Hu, H. Yang, D. Pan, H. Wang, J. Tian, S. Zhang, X. Wang, A. A. Volinsky, Heat treatment effects on microstructure and magnetic properties of Mn–Zn ferrite powders. J. Magn. Magn. Mater. Vol. 322, pp. 173 (2010).

[2] M. Syue, F. Wei, C. Chou, C. Fu, Magnetic, dielectric, and complex impedance properties of nanocrystalline Mn–Zn ferrites prepared by novel combustion method, Thin Solid Films, vol. 519, pp. 8303 (2011).

[3] M. Syue, F. Wei, C. Chou, C. Fu, Magnetic and electrical properties of Mn–Zn ferrites synthesized by combustion method without subsequent heat treatments, J. Appl. Phys., vol. 109, pp. 07A324 (2011).

[4] Th. H. de Keijser, J. I. Langford, E. J. Mittemeijer, A. B. P. Vogels, Use of the Voigt function in a single-line method for the analysis of X-ray diffraction line broadening. J. Appl. Cryst., vol. 15, pp. 308 (1982).

[5] B. E. Warren, B. L. Averbach, The Effect of Cold Work Distortion on X-Ray Patterns. J. Appl. Phys., vol.21, pp. 595 (1950).

[6] A. Coelho. Topas Academic Version 4.1. Computer Software, Topas Academic, Coelho Software, Brisbane, 2007.

[7] C. E. Krill, R. Birringer, Estimating grain-size distributions in nanocrystalline materials from X-ray diffraction profile analysis, Philos. Mag. A., vol. 77, pp. 621 (1998).

[8] C. Rath, S. Anand, R. P. Das, K. K. Sahu, S. D. Kulkarni, S. K. Date, N. C. Mishra, Dependence on cation distribution of particle size, lattice parameter, and magnetic properties in nanosize Mn-Zn ferrite, J. Appl. Phys., vol. 91, pp. 2211 (2002).